Improvement of the Efficiency of Plasma Display Panels by Combining Waveform and Cell Geometry Design

G. Veronis, *Member, IEEE,* and U. S. Inan, *Senior Member, IEEE*

***Abstract*—A two-dimensional self-consistent simulation model is used to investigate the effect of several different sustaining voltage waveforms on the luminous efficiency of plasma display panel (PDP) cells. We first show that such a model can reproduce all the major trends of experimental display measurements concerning the effect of waveform on PDP efficiency. We then use this model to put forth new high-efficiency PDP designs. A new sustaining waveform combining assistant voltage pulses with asymmetric pulse driving results in $\sim 25\%$ maximum increase in efficiency within the voltage margin of the cell. A new plasma display using combined waveform and electrode designs is determined to have a maximum increase in efficiency of $\sim 40\%$.**

***Index Terms*—Dielectric barrier discharges, discharge simulation, microdischarge plasmas, plasma display panel (PDP).**

I. Introduction

THE PLASMA display panel (PDP) is the leading candidate in the competition for large-size, high-brightness, high-contrast-ratio flat panel displays, suitable for high definition television (HDTV) wall-mounted monitors [1]–[3]. Its advantages include high resolution, wide viewing angle, low weight, and simple manufacturing process for fabrication. Recent progress in PDP technology development and manufacturing has been remarkable [4], [5].

Typical color plasma displays consist of two glass plates, each with parallel electrodes deposited on their surfaces. The electrodes are covered with a dielectric film. The plates are sealed together with their electrodes at right angles, and the gap between the plates is first evacuated and then filled with an inert gas mixture. A protective MgO layer is deposited above the dielectric film. The primary role of this layer is to decrease the breakdown voltage due to the high secondary electron emission coefficient of MgO. The ultraviolet (UV) photons emitted by the discharge hit the phosphors deposited on the walls of the PDP cell and are converted into visible photons. Each cell contains a specific type of phosphor that emits one primary color, namely red, green, or blue.

The most common type of color plasma display is the coplanar-electrode PDP. In this PDP type, each cell is formed by the intersection of a pair of transparent sustain electrodes on the front plate, and an address electrode on the back plate. During operation, a periodic voltage with a frequency of 50–350 kHz is continuously applied between each pair of sustain electrodes. The amplitude of the sustain voltage is kept below the breakdown voltage. A cell is turned on by applying a write voltage pulse between the address electrode and one of the sustain electrodes. The discharge which is thus initiated results in the deposition of surface charge on the dielectric layers covering these two electrodes. The superposition of the electric field induced by the deposited surface charge and of the electric field of the applied sustaining voltage results in the ignition of sustain discharges between the pair of sustain electrodes.

One of the most critical remaining issues in ongoing PDP research is the improvement of the luminous efficiency, which is still low compared to conventional cathode ray tube (CRT) displays. The research for increased efficiency has been extremely vigorous as evidenced by the fast increase in the number of papers published in this domain [3]. A number of different approaches have been pursued to improve the efficiency of the standard coplanar-electrode PDP design including the modification of the electrode shape and of the cell geometry [4]–[8], the optimization of the gas mixture composition [9]–[11], and the use of novel materials [3].

The PDP efficiency can also be increased by modifying the voltage waveforms applied to the electrodes of the display during operation. A large number of alternative waveforms with improved efficiency have been proposed [12]–[21]. Most of them are based on alternative driving voltage schemes with frequencies in the conventional 50–350 kHz range [12]–[18]. Recently, the use of radio-frequency (RF) voltages around 50 MHz has been proposed to replace the conventional sustaining voltage [19], [20]. Other technological challenges must, however, be overcome before RF waveforms become practical for PDP applications [3].

In this paper, we consider several different sustaining voltage waveforms with frequencies in the conventional range, and investigate the effect of the sustaining waveform on the efficiency of the PDP cell. We propose a new sustaining waveform based on combination of two different waveform schemes. We also

Manuscript received December 16, 2003; revised October 28, 2004. This work was supported in part by the Office of Technology Licensing of Stanford University under Grant 127P316, by the National Science Foundation under Grant ATM-9908766, and in part by the Center for Integrated Systems at Stanford University.

G. Veronis is with the Center for Integrated Systems, Stanford University, Stanford, CA 94305 USA.

U. S. Inan is with the Space, Telecommunications, and Radioscience Laboratory, Stanford University, Stanford, CA 94305 USA.

Digital Object Identifier 10.1109/TPS.2004.841802

propose a new plasma display design involving a combination of waveform and electrode designs. We quantitatively demonstrate that these new designs achieve higher luminous efficiency when compared with conventional designs.

PDP cells are small (cell height is $\sim 150\ \mu\mathrm{m}$) and provide limited access for diagnostic measurements. As a result, experimental studies of the transient plasma discharges in PDPs are extremely difficult, and computer-based modeling is currently essential for understanding PDP physics and optimizing its operation. Simulation results are used very effectively to provide directions for future PDP design. In this paper, we use a two-dimensional (2-D) self-consistent model to simulate the microdischarges in PDP cells. We first show that such a model can reproduce all the major trends of experimental display measurements concerning the effect of sustaining waveform on PDP efficiency. We then use this model to suggest new high-efficiency PDP designs.

This paper is organized as follows. The two-dimensional self-consistent simulation model is briefly described in Section II. The results obtained using this model for the various waveform and cell geometry designs are presented in Section III. Finally, our conclusions are summarized in Section IV.

II. Model Description

We provide only a brief description of the self-consistent fluid model used to simulate the microdischarges in the PDP cell since this model has been described in detail elsewhere [6], [22].

For each species s, the spatial and temporal variations of the density are calculated by solving the continuity equation

$$\frac{\partial n_s}{\partial t} + \boldsymbol{\nabla} \cdot \boldsymbol{\Gamma}_s = S_s \tag{1}$$

where n_s is the number density, $\boldsymbol{\Gamma}_s$ is the particle flux, and S_s is the source term determined by the particle production and loss processes. We consider electrons, atomic $(\mathrm{Ne}^+, \mathrm{Xe}^+)$ and molecular $(\mathrm{Ne}_2^+, \mathrm{Xe}_2^+, \mathrm{NeXe}^+)$ ions, and excited species [Ne_m^*, $\mathrm{Xe}^*(^3\mathrm{P}_1)$, $\mathrm{Xe}^*(^3\mathrm{P}_2)$, Xe^{**}, $\mathrm{Xe}_2^*(\mathrm{O}_u^+)$, $\mathrm{Xe}_2^*(^3\Sigma_u^+)$, $\mathrm{Xe}_2^*(^1\Sigma_u^+)$] for a Ne–Xe mixture.

We use the drift-diffusion equation as an approximation to the momentum equation

$$\boldsymbol{\Gamma}_s = \mathrm{sgn}(q_s) n_s \mu_s \mathbf{E} - D_s \nabla n_s \tag{2}$$

where q_s is the particle charge, μ_s is the particle mobility, $\mathbf{E}$ is the electric field, and D_s is the diffusion coefficient.

The electric field within the cell is self-consistently calculated by solving Poisson's equation

$$\nabla \cdot (\varepsilon \mathbf{E}) = \sum_s q_s n_s \tag{3}$$

where ε is the dielectric permittivity.

Electron impact reaction rates and transport coefficients are assumed to be functions of the electron mean energy, which is determined by solving the electron energy equation

$$\frac{\partial n_\varepsilon}{\partial t} + \boldsymbol{\nabla} \cdot \boldsymbol{\Gamma}_\varepsilon = S_\varepsilon \tag{4}$$

where $n_\varepsilon = n_e \overline{\varepsilon}$ is the electron energy density, n_e is the electron density, $\overline{\varepsilon}$ is the electron mean energy, $\boldsymbol{\Gamma}_\varepsilon$ is the electron energy flux, and S_ε is the electron energy source term given by

$$\boldsymbol{\Gamma}_\varepsilon = -\frac{5}{3} n_\varepsilon \mu_e \mathbf{E} - \frac{5}{3} D_e \nabla n_\varepsilon \tag{5}$$

and

$$S_\varepsilon = -e \boldsymbol{\Gamma}_e \cdot \mathbf{E} - n_e \sum_i \nu_i \varepsilon_i. \tag{6}$$

The summation in the second term is over all of the electron impact reactions with occurrence frequency ν_i, with ε_i being the corresponding electron loss energy. We use the more accurate electron energy equation method instead of the local field approximation (LFA) for electron impact reaction rates and transport coefficients because the LFA introduces large errors in the calculation of the discharge efficiency [22], [23].

We use a finite difference method to solve the system of partial differential equations. The continuity equations and the electron energy equation are solved implicitly, while semi-implicit methods are used for the integration of the coupled continuity and field equations, and for the source term in the electron energy equation. The electron impact ionization and excitation frequencies, as well as the electron mobility, are calculated using the Boltzmann code ELENDIF [24]. Electron–atom collision cross sections for Ne and Xe are taken from the SIGLO Series [25]. Rate coefficients for Penning ionization, dimer ions formation, charge exchange, recombination, and neutral kinetics reactions, as well as excited species lifetimes are taken from Meunier *et al.* [26]. Secondary electron emission coefficients are the same as in Veronis and Inan [22].

As in [26], a Holstein escape factor is used to describe the lengthening of the apparent lifetime of the resonant state $\mathrm{Xe}^*(^3\mathrm{P}_1)$ due to radiation trapping. A more detailed Monte Carlo simulation of the resonance radiation transport by Hagelaar *et al.* [27] showed that this approach is good enough, and that the escape factor estimated from Holstein's theory was in good agreement with the value deduced from the Monte Carlo simulation.

Electron and ion diffusion coefficients are determined using the Einstein relation

$$\frac{D}{\mu} = \frac{k_B T}{e} \tag{7}$$

where k_B is the Boltzmann constant, T is the particle temperature, and e is the elementary charge. The ion temperature is assumed to be equal to the gas temperature.

In order to calculate the visible light output of the PDP cell, we implement a radiation transport model, similar to the one described in [28].

III. Results

A. Cell Geometry and Calculation of Efficiency

The geometry of the standard coplanar-electrode PDP cell used in the simulations is shown in Fig. 1(a). The cell consists of two sustain electrodes, X and Y, separated from the gas by a dielectric layer. An MgO layer is deposited on the dielectric

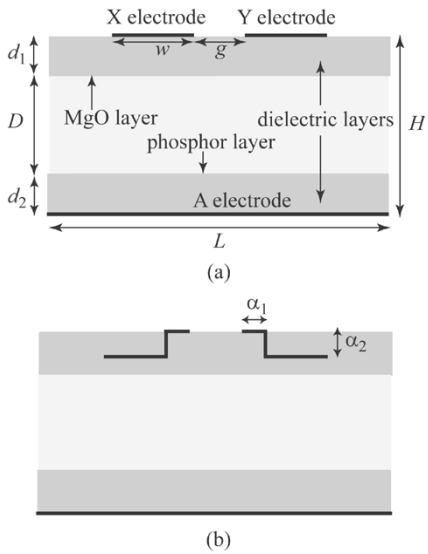

Fig. 1. (a) Schematic of the standard coplanar-electrode PDP cell. (b) Schematic of the electrode-shaping geometry.

film. The bottom of the cell consists of the address electrode A, separated from the gas by a dielectric layer with a phosphor layer on top. The output window of the device is the top side of the upper dielectric layer, noting that the sustain electrodes are transparent. In all cases, the gas mixture filling the region between the dielectrics is a Ne–Xe mixture with 4% Xe at a pressure of 500 torr. The height and width of the cell are $H = 210\ \mu\text{m}$ and $L = 1260\ \mu\text{m}$, respectively. Other parameter values are $g = 60\ \mu\text{m}$, $w = 380\ \mu\text{m}$, $d_1 = 30\ \mu\text{m}$, $d_2 = 30\ \mu\text{m}$, and $\varepsilon_r = 10$, where g is the electrode gap length, w is the sustain electrode width, d_1, d_2 are the lengths of the upper and lower dielectric layers, respectively, and ε_r is the dielectric constant.

In Fig. 1(b), we show a PDP cell geometry with modified shape of sustain electrodes, which for brevity will heretofore be referred to as the electrode-shaping geometry. This design was recently proposed by Veronis and Inan [6] as an efficient cell geometry design. For the electrode-shaping geometry used in the simulations we have $a_1 = 100\ \mu\text{m}$ and $a_2 = 20\ \mu\text{m}$; all other parameters being the same as in the standard PDP cell.

The UV photons, which excite the phosphors, are emitted by certain excited states of Xe [$\text{Xe}^*(^3\text{P}_1)$ (resonant state) at 147 nm, $\text{Xe}_2^*(\text{O}_u^+)$ at 150 nm, $\text{Xe}_2^*(^3\Sigma_u^+)$ and $\text{Xe}_2^*(^1\Sigma_u^+)$ at 173 nm (excimer states)] [26]. The excited phosphors, in turn, emit visible photons. We define the visible light generation efficiency of the cell as the ratio of total visible photon energy, which reaches the output window, to the total energy dissipated during a sustaining period

$$\eta = \frac{\int_T dt \int_{S_{\text{out}}} ds \mathbf{\Gamma}_{\text{ph}} \varepsilon_{\text{ph}}}{\int_T dt \int_V dv \left(\mathbf{J}_e + \sum_{i=1}^{N_{\text{ion}}} \mathbf{J}_{\text{ion}\,i} \right) \cdot \mathbf{E}} \tag{8}$$

where $\mathbf{\Gamma}_{\text{ph}}$ is the number of visible photons reaching the output window per unit area and per unit time, ε_{ph} is the visible photon energy, and $\mathbf{J}_e$, $\mathbf{J}_{\text{ion}\,i}$ are the electronic and ionic current (of ion i) respectively. We take the visible photon wavelength to be 550 nm. We calculate the efficiency of the PDP cell in the periodic steady state, typically involving the application of at least six sustaining pulses.

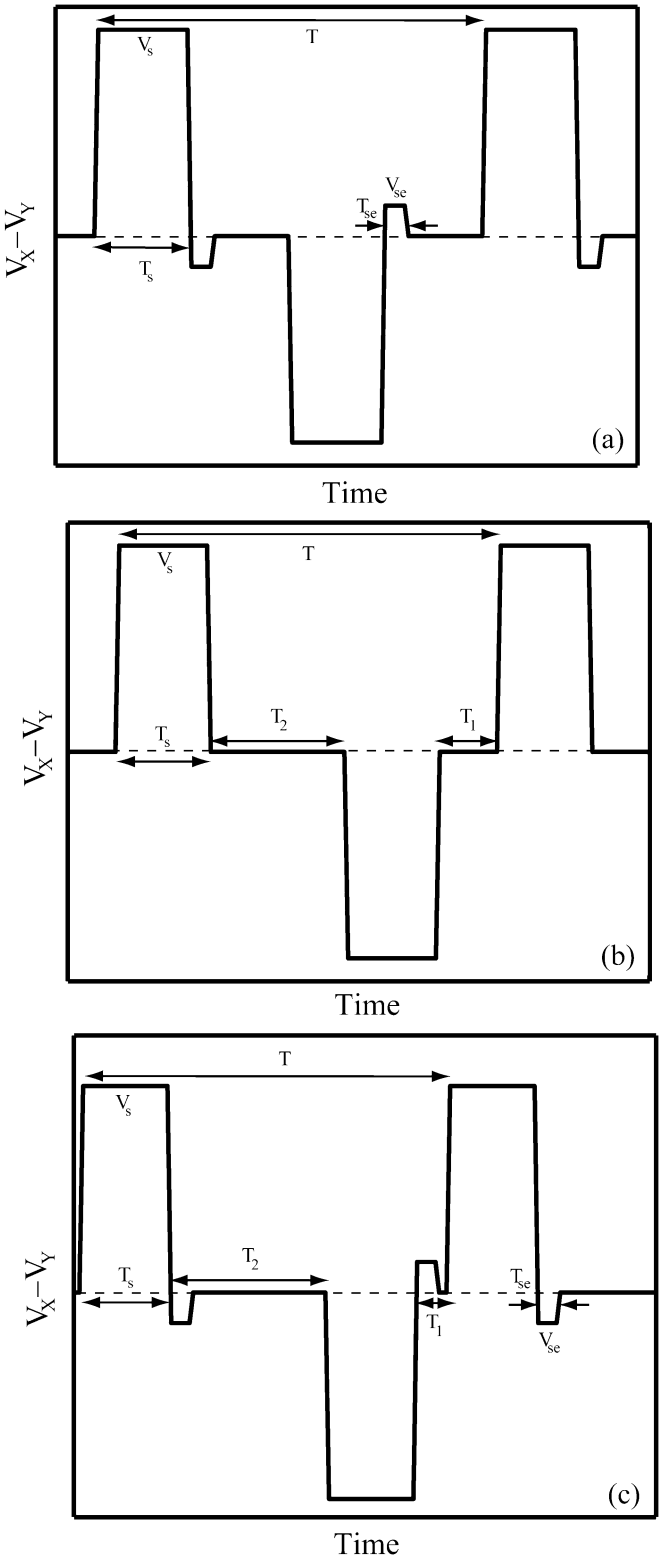

Fig. 2. (a) Self-erase discharge waveform used in the simulations. In all cases, the waveform period is $T = 10\ \mu\text{s}$. Sustaining pulses of magnitude V_S and duration T_S are followed by assistant pulses of opposite polarity with magnitude V_{se} and duration T_{se}. (b) Asymmetric pulse waveform used in the simulations. In all cases, the waveform period is $T = 10\ \mu\text{s}$. In the asymmetric pulse waveform, the pulse-off time ratio is $T_1/T_2 \neq 1$. (c) Combination of the self-erase discharge and asymmetric pulse waveforms. Waveform period is $T = 10\ \mu\text{s}$.

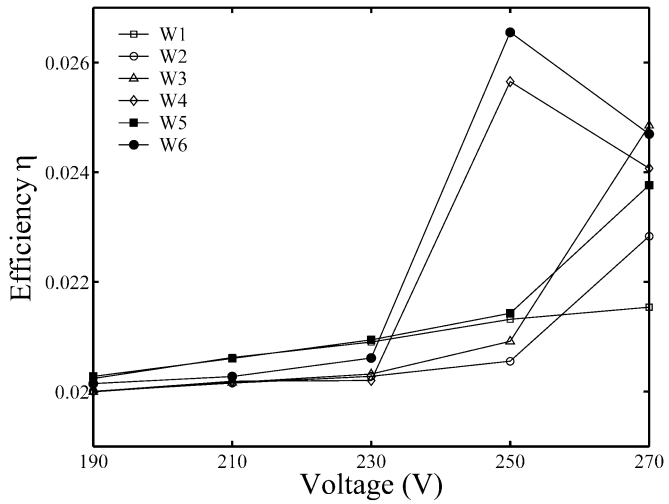

Fig. 3. Visible light generation efficiency η as a function of sustaining voltage V_S for various sustaining waveforms. Results are shown for the standard coplanar-electrode geometry [Fig. 1(a)]. Sustaining frequency is 100 kHz in all cases [$T = 10\ \mu$s in Fig. 2(a)–(c)] and the rise and fall times of all pulses are 100 ns. For our reference waveform W1, we have $T_s = T/2 = 5\ \mu$s, $T_{\rm se} = 0$. In all other cases, $T_s = 2.5\ \mu$s. For waveforms W2, W3, and W4, we have $V_{\rm se} = 0$, 10 V, 20 V, respectively, and $T_{\rm se} = 700$ ns [Fig. 2(a)]. For waveform W5, we have $T_1 = 0.2\ \mu$s, $T_2 = 4.8\ \mu$s [Fig. 2(b)]. Finally, waveform W6 combines characteristics of both self-erase discharge and asymmetric pulse waveforms. For W6, we have $V_{\rm se} = 20$ V, $T_{\rm se} = 700$ ns, and $T_1 = 0.8\ \mu$s, $T_2 = 4.2\ \mu$s [Fig. 2(c)].

B. Self-Erase Discharge Waveform

As we mentioned above, the focus of this paper is the effect of the sustaining waveform on the efficiency of the PDP cell. We consider several different sustaining voltage waveforms. The sustaining frequency is 100 kHz in all cases [$T = 10\ \mu$s in Fig. 2(a)–(c)] and the rise and fall times of all pulses are 100 ns. The effect of waveform frequency and risetime on the efficiency of the device has been investigated elsewhere [23] and will not be discussed here. However, it should be noted that our model results reproduce the trends of dependences on frequency and risetime as reported by Hagelaar *et al.* [23].

Fig. 3 shows the efficiency η as a function of sustaining voltage V_S for several different sustaining waveforms. The efficiency is calculated using (8) for voltages within the voltage margin of the cell defined by the minimum sustaining voltage $V_{S\min}$ and the firing voltage V_f [29]. The calculation of $V_{S\min}$ and $V_{\rm f}$ is done as described in Veronis and Inan [22]. We note that usually in PDP models, the required sustain voltages are slightly higher (20%) than in reality [23]. Our reference standard waveform (W1 in Fig. 3) is characterized by $T_s = T/2$, $T_{se} = 0$ [Fig. 2(a)]. We observe that for W1, the calculated efficiency η has a weak dependence on the sustaining voltage V_S (slightly increases as the voltage increases). We note that several experimental results concerning the dependence of luminous efficiency on the applied voltage have been previously reported. Oversluizen *et al.* [11] report a fairly flat efficiency as a function of voltage for a Ne–Xe mixture with 3.5% Xe at a pressure of 487 torr. Chung *et al.* [30] report a decreasing efficiency as a function of voltage for a Ne–Xe mixture with 4% Xe at a pressure of 600 torr. Finally, Hagelaar *et al.* [23] report an increasing efficiency as a function of voltage for a Ne–Xe mixture with 10% Xe. We note, however, that the 10% Xe percentage in this case is substantially higher than the one in our simulation mixture, so that comparison is not meaningful.

In recent years, a new class of sustaining waveforms, known as self-erase discharge waveforms, has been proposed by several experimenters to increase the efficiency of the PDP cell [12], [13], [15], [17], [18]. The main idea in all these voltage schemes is to promote a "self-erase" discharge, which partially erases the surface charge deposited on the upper dielectric by the previous discharge. In Fig. 2(a), we show the self-erase discharge sustaining waveform used in our simulations [13]. In all cases, $T_s = 2.5\ \mu$s, $T_{\rm se} = 700$ ns. In Fig. 3, we show the efficiency η as a function of the sustaining voltage V_S for $V_{\rm se} = 0$, 10, 20 V (waveforms W2, W3, W4, respectively) for the standard coplanar-electrode geometry [Fig. 1(a)]. We observe that the efficiency of the self-erase waveform is significantly higher than the efficiency of the standard waveform at high sustaining voltages. There is an increase in efficiency even for $V_{\rm se} = 0$ V. As $V_{\rm se}$ is increased, higher efficiency is observed over a wider range of sustaining voltages, and the maximum increase in efficiency is larger. For $V_{\rm se} > 20$ V, the operation of the cell becomes unstable over a sustaining voltage range within the voltage margin. All these trends are consistent with results of experiments [13].

The visible light generation efficiency defined in (8) can also be written as [6]

$$\begin{aligned}\eta &= \eta_1\eta_2\eta_3\eta_4\\ \eta_1 &= \frac{\varepsilon_{\rm el}}{(\varepsilon_{\rm el}+\varepsilon_{\rm ion})}\\ \eta_2 &= \frac{\varepsilon_{\rm exc}}{\varepsilon_{\rm el}}\\ \eta_3 &= \frac{\varepsilon_{\rm UV}}{\varepsilon_{\rm exc}}\\ \eta_4 &= \frac{\varepsilon_{\rm vis}}{\varepsilon_{\rm UV}}\end{aligned} \tag{9}$$

where $\varepsilon_{\rm el}$ and $\varepsilon_{\rm ion}$ are the total energies dissipated per period by electrons and ions, respectively, $\varepsilon_{\rm exc}$ is the total energy lost by electrons per period in collisions that lead to the production of UV emitting excited states of xenon, $\varepsilon_{\rm UV}$ is the total UV emitted energy per period, and $\varepsilon_{\rm vis}$ is the total visible light energy reaching the output window. Physically, η_1 is the efficiency of the discharge in heating the electrons, η_2 is the efficiency of electrons in producing ultaviolet (UV) emitting states of xenon, and η_3 is the efficiency of emission of UV photons by xenon excited atoms and molecules. Finally, η_4 is an additional factor in the overall visible light generation efficiency η, related to the efficiency of transport of UV photons to the phosphor layer and of the visible photons to the output window, and to the UV-to-visible conversion efficiency of the phosphor. The simulation results indicate that the effect of the sustaining waveform and cell geometry on η_3 is small, because η_3 is mainly determined by the gas mixture composition. Similarly, the effect of the sustaining waveform and cell geometry on η_4 is small [6]. We therefore focus our attention on the excitation efficiency defined as

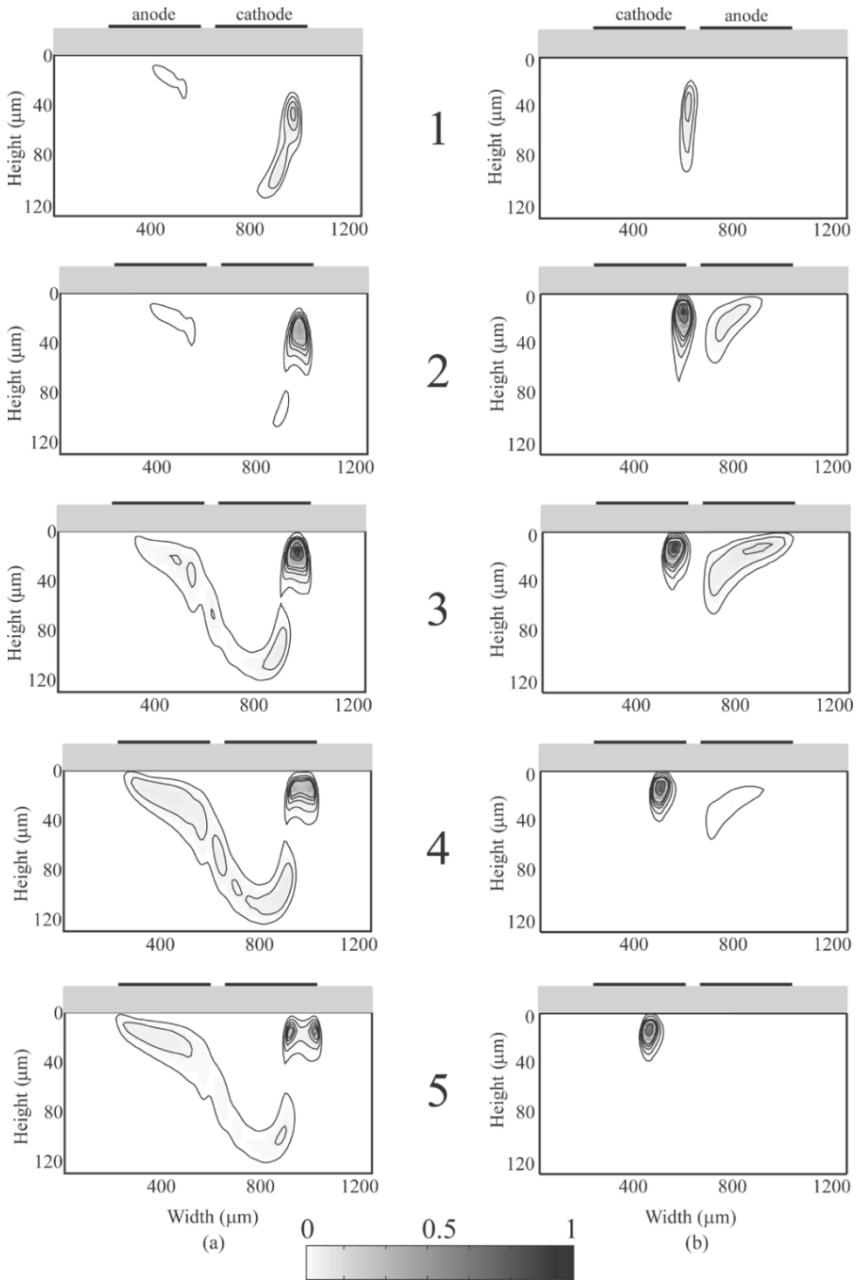

Fig. 4. (a) Normalized power spent for xenon excitation $\bar{p}_{\rm exc}$, integrated over 4.8 ns consecutive time intervals, for the self-erase discharge waveform [Fig. 2(a)] applied to the standard coplanar-electrode geometry [Fig. 1(a)]. Results are shown for waveform W3 (Fig. 3) and $V_S = 270$ V. Starting time for integration is 759 ns after the application of a sustaining pulse V_S. (b) Normalized power spent for xenon excitation $\bar{p}_{\rm exc}$, integrated over 8.5-ns consecutive time intervals, for our reference standard waveform W1 (Fig. 3) applied to the standard coplanar-electrode geometry [Fig. 1(a)]. Results are shown for $V_S = 270$ V. Starting time for integration is 87 ns after the application of a sustaining pulse V_S. Maximum in the gray scale corresponds to 4.09 $\times 10^7$ m^{-2}. Contours correspond to 0.02, 0.05, 0.1, 0.15, 0.2, 0.5, 0.8 of the maximum value. Note the different vertical scale in each plot. In all cases, height is measured from the MgO layer surface.

$\eta_{\rm exc} = \eta_1 \eta_2$, representing the components of the overall efficiency most significantly affected by geometry and waveform variations. The excitation efficiency is therefore given by

$$\eta_{\rm exc} = \frac{\int_T dt \int_V dv \sum_{i=1}^{N_{\rm exc}} n_e \nu_i^* \varepsilon_{{\rm exc}\,i}}{\int_T dt \int_V dv \left(\mathbf{J}_e + \sum_{i=1}^{N_{\rm ion}} \mathbf{J}_{{\rm ion}\,i} \right) \cdot \mathbf{E}} \tag{10}$$

where ν_i^* is the excitation frequency of excited state of Xe i which leads through a series of reactions to UV photon production, and $\varepsilon_{{\rm exc}\,i}$ is the corresponding electron loss energy.

We may note that the excitation efficiency can also be written as [22]

$$\eta_{\rm exc} = \int_V dv \left[\int_T dt \frac{p_{\rm exc}}{\varepsilon_{\rm tot}} \right] \tag{11}$$

where $p_{\rm exc} = \sum_{i=1}^{N_{\rm exc}} n_e \nu_i^* \varepsilon_{{\rm exc}\,i}$, and $\varepsilon_{\rm tot} = \int_T dt \int_V dv p$, where $p = (\mathbf{J}_e + \sum_{i=1}^{N_{\rm ion}} \mathbf{J}_{{\rm ion}\,i}) \cdot \mathbf{E}$. Equation (11) suggests that the excitation efficiency $\eta_{\rm exc}$ is obtained by integrating (over space and time) the power spent for xenon excitation ($p_{\rm exc}$), normalized by the total energy dissipated in the discharge ($\varepsilon_{\rm tot}$). For purposes of brevity, this quantity, which is directly related to the

excitation efficiency, will heretofore be referred to as the normalized power spent for xenon excitation $\tilde{p}_{\rm exc}$. In Fig. 4(a) and (b), we show snapshots of $\tilde{p}_{\rm exc}$, integrated over time, for the self-erase discharge waveform [Fig. 2(a)] and our reference standard waveform respectively, applied to the standard coplanar-electrode geometry [Fig. 1(a)]. We observe that the discharge path is much longer in the self-erase waveform case. It has been shown in earlier work that the wider the discharge area, the higher the efficiency [22]. We also observe that in the self-erase waveform case, the initial discharge path is formed below the outer part of the sustain electrode in the cathode region [snapshots 1, 2 of Fig. 4(a)]. In the standard waveform case, the initial discharge path is formed below the inner part of the electrode, where the electric field is higher [snapshots 1, 2 of Fig. 4(b)] [6]. The increased efficiency resulting from the use of the self-erase waveform is due to this difference in the discharge paths. In order to interpret this difference, we focus our attention on the surface charge density deposited on the upper dielectric before the initiation of the discharge. We observe that in the self-erase waveform case, only the portion of the dielectric below the outer part of the cathode is covered with negative charge [Fig. 5(a)]. In the standard waveform case, the charge distribution is almost uniform below the cathode [Fig. 5(a)]. The reason for this difference is that in the self-erase waveform case the assistant negative voltage pulse of magnitude $V_{\rm se}$ [Fig. 2(a)] triggers a self-erase discharge between the two sustain electrodes that partially erases the surface charge deposited by the previous main discharge. The path of the self-erase discharge is formed below the inner part of the cathode, where the electric field is higher and, consequently, the surface charge below this inner part is erased. If $V_{\rm se}$ is low enough ($V_{\rm se} < 20$ V for our simulation case), the surface charge is only partially erased. As a result, when the subsequent main sustaining pulse of magnitude V_S is applied, the maximum field path is toward the outer part of the cathode, which is covered with negative surface charge. Thus, the discharge path is longer and the discharge more efficient. If $V_{\rm se} > 20$ V, the self-erase discharge almost completely erases the negative charge deposited by the previous main discharge, so that the device is turned off and the cell operation becomes unstable. We note that in the standard waveform case all sustaining discharges have the same intensity and efficiency. In the self-erase waveform case, we have main discharges and self-erase discharges with different intensities [13]. According to the simulation results, it is the former that are more efficient, resulting in higher overall efficiency of the device in the steady state of operation. In summary, in the self-erase waveform case, a self-erase discharge partially erases the surface charge on the upper dielectric resulting in a longer and consequently more efficient path for the main discharge. We note that this physical mechanism, which results in increased efficiency, was not identified in the experimental work that introduced this self-erase waveform [13]. Such mechanisms can only be identified through computer simulations of or sophisticated diagnostic measurements within the microscopic PDP cells.

We note that the spatiotemporal variation of the surface charge distribution was recently measured for the first time

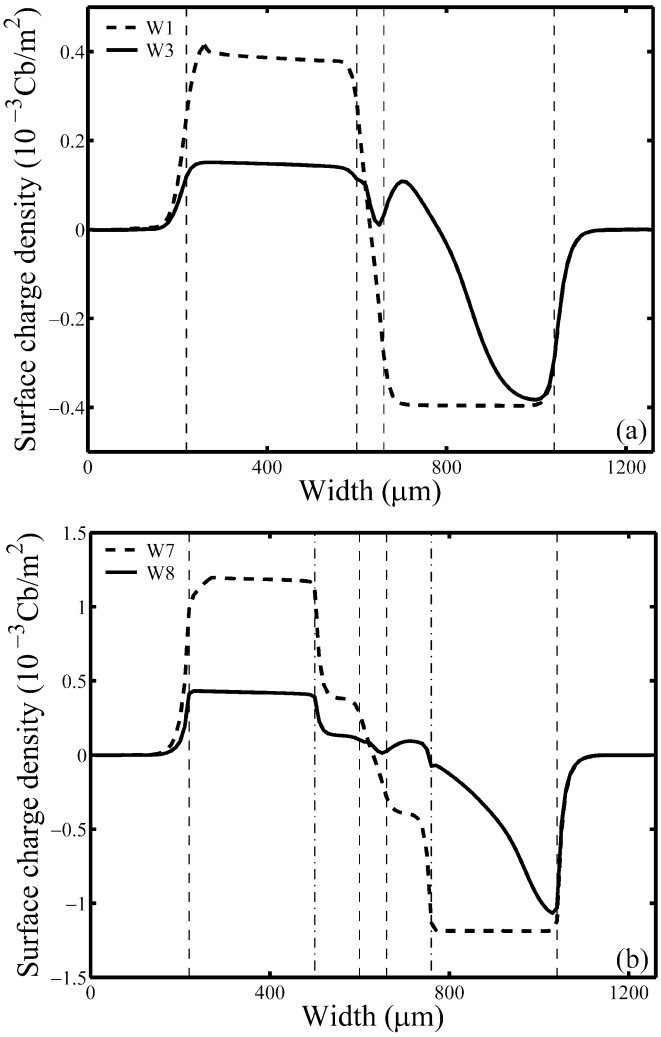

Fig. 5. (a) Surface charge density on the upper dielectric layer for waveforms W1 and W3 (Fig. 3). Results are shown for the standard coplanar-electrode geometry [Fig. 1(a)] before the initiation of a main discharge caused by a sustaining voltage pulse of magnitude V_S (Fig. 2). Sustaining voltage is $V_S = 270$ V. (b) Surface charge density on the upper dielectric layer for waveforms W7 and W8 (Fig. 8). Results are shown for the electrode-shaping geometry [Fig. 1(b)] before the initiation of a main discharge caused by a sustaining voltage pulse of magnitude V_S (Fig. 2). Sustaining voltage is $V_S = 270$ V. Positions of electrodes are shown with dashed lines. Dash-dot lines correspond to the positions where the two horizontal segments of the shaped electrodes are connected.

using the longitudinal electrooptic amplitude modulation method [31]. Some aspects of the measured variation of surface charge are not reproduced by our simulation model. In particular, the measured surface charge density deposited on the upper dielectric before the initiation of the discharge was found to be nonuniform in the standard waveform case [31]. In our simulation results, the charge distribution is almost uniform below the cathode, as mentioned above [Fig. 5(a)]. However, the basic characteristics of the measured spatiotemporal variation of surface charge are well reproduced by our model. More specifically, it was found in the experiment that the discharge is ignited from the inner edge of the anode and then moves to the cathode. In addition, electron surface charge on the cathode is annihilated from the inner to the outer side of the electrode. Finally, it was found that the ion surface charge

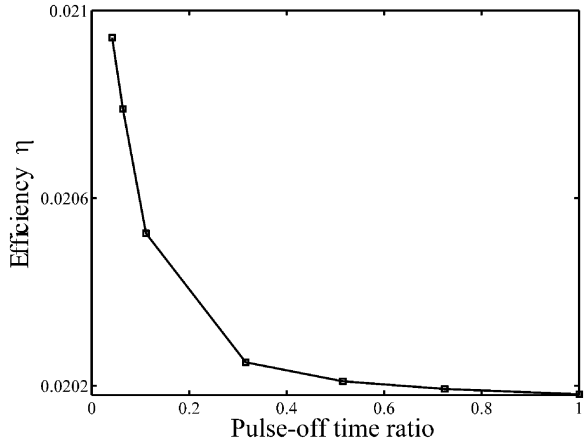

Fig. 6. Visible light generation efficiency η as a function of the pulse-off time ratio T_1/T_2 for the asymmetric pulse waveform (Fig. 2(b)). Results are shown for the standard coplanar-electrode geometry (Fig. 1(a)). In all cases, $T = 10\ \mu$s, $T_s = 2.5\ \mu$s, so that $T_1 + T_2 = 5\ \mu$s. Rise and fall times of all pulses are 100 ns. Sustaining voltage is $V_S = 230$ V.

near the discharge gap decreases faster than the electron surface charge [31]. Our simulation results are in good agreement with all these experimental findings. We therefore believe that our interpretation of the increased efficiency of the self-erase discharge waveform based on the calculated surface charge distributions is valid.

C. Asymmetric Pulse Waveform

Recently, a new type of sustaining waveform, referred to as asymmetric pulse driving, has been used in experimental work, resulting in enhanced PDP efficiency [14]. In Fig. 2(b), we show the asymmetric pulse sustaining waveform used in our simulations [14]. In all cases, $T_s = 2.5\ \mu$s, $T = 10\ \mu$s. In the standard waveform case, we have $T_1 = T_2$ ($T_1 = T_2 = 0$ in our reference case W1 in Fig. 3). In the asymmetric pulse case, we vary the parameter T_1/T_2 which will heretofore be referred to as the pulse-off time ratio [14]. In Fig. 6, we show the efficiency η as a function of the pulse-off time ratio T_1/T_2. We observe that the efficiency increases as the pulse-off time ratio decreases, with the model once again correctly reproducing the experimental trends [14]. For the specific value of V_S in Fig. 6, the maximum increase in efficiency is relatively small. In Fig. 3, we show the dependence of efficiency on the sustaining voltage V_S for a constant value of the pulse-off time ratio (waveform W5). The dependence of η on V_S, and the maximum achievable increase in η are similar to the self-erase waveform case.

The improved performance of the asymmetric pulse waveform can be interpreted based on the results shown in Fig. 7(a) and (b). Here we show the integrated density of xenon metastable atoms and the total volume charge in the cell as a function of time for different values of the pulse-off time ratio T_1/T_2. We observe that the xenon metastable atoms decay rather slowly compared to charged species and their dynamics depend on the temporal position of the applied pulses [14]. We found that their influence on the discharge dynamics through stepwise ionization processes is significant for small values of the pulse-off time ratio. The increased density of metastable atoms, as the pulse-off time ratio decreases, leads also to intensified UV emission and therefore higher efficiency.

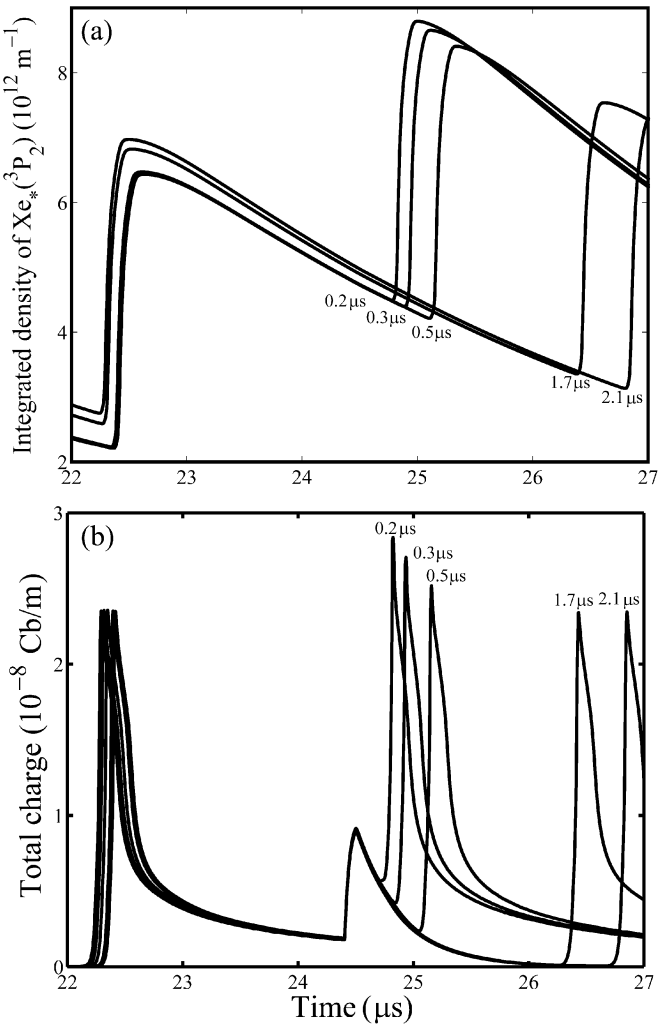

Fig. 7. (a) Integrated density of xenon metastable atoms and (b) total volume charge in the cell as a function of time for different values of T_1 for the asymmetric pulse waveform [Fig. 2(b)]. In all cases, $T = 10\ \mu$s, $T_s = 2.5\ \mu$s, so that $T_1 + T_2 = 5\ \mu$s. Rise and fall times of all pulses are 100 ns. Sustaining voltage is $V_S = 230$ V.

When a discharge occurs in the cell, a cathode region with positive charge and an almost neutral plasma region are formed so that the total volume charge is positive [26]. After the discharge, charge densities in the cell decrease with time constants determined by ambipolar diffusion and recombination processes. In Fig. 7(b), we observe that in all cases, a discharge occurs at $t \simeq 22.2\ \mu$s shortly after the application of a sustaining pulse of magnitude V_S at $t = 22\ \mu$s. After the discharge, the volume charge and the electric field in the cathode region decay. The electric field induced by the deposited surface charge opposes the electric field of the applied sustaining voltage. At $t = 24.5\ \mu$s, the 2.5-μs sustaining pulse is turned off and the electric field in the gap increases due to the presence of the uncompensated surface charge. The increase in the electric field results in increased deposition of the electrons on the surface of the dielectrics (due to their much higher mobility) and therefore, an increased volume charge in the cell. After $t = 24.5\ \mu$s, the charge in the cathode region decays again. We observe that for $T_1 > 1\ \mu$s, the volume charge decays almost completely before the application of the next sustaining pulse so that the asymmetric pulse driving has almost no effect.

However, for $T_1 < 1\ \mu$s, the volume charge due to the previous discharge does not decay completely before the next sustaining pulse is applied, resulting in a more intense and more efficient discharge.

In [14], it was suggested that charged particles in the discharge volume decay too fast to affect the sequent discharge. On the contrary, our simulation results suggest that volume charges have a significant effect on the decay dynamics. We note that we use a relatively high sustaining frequency (100 kHz) so that for small pulse-off time ratios, charged particles do not decay completely before the next pulse is applied. At lower sustaining frequencies, as those used in the experiment [14], the effect of charged particles is negligible and the efficiency improvement is due to the metastables.

D. New PDP Designs

In the previous two subsections, we used the 2-D model to simulate nonstandard sustaining waveforms, which were previously shown (in experiments) to increase the efficiency of a plasma display. We showed that the model can reproduce the major trends of these experiments and furthermore proves to be useful in physical understanding of the mechanisms leading to the improved performance of these waveforms. In this section, we use the model to propose new efficient PDP designs.

In Fig. 3, we show the efficiency η as a function of the sustaining voltage V_S for a new waveform design (W6), which combines the characteristics of self-erase discharge and asymmetric pulse waveforms [Fig. 2(c)]. We use assistant pulses $(T_{\rm se} = 700\ {\rm ns})$ to promote the self-erase discharge combined with asymmetric pulse driving $(T_1 = 0.8\ \mu{\rm s})$. We observe that the maximum achievable increase in η is higher for this new waveform when compared to the self-erase discharge and asymmetric pulse waveforms. For our simulation conditions, the maximum increase in η (with respect to the reference W1) is found to be $\sim 25\%$. Thus, our results suggest that a combination of these efficient waveform designs can result in even further increase in efficiency. It is interesting to note that such was not the case when individually efficient geometry designs were combined in our previous work [6].

In Fig. 8, we show η for the electrode-shaping geometry of Fig. 1(b) as a function of V_S for several different sustaining waveforms. We observe that when our reference standard waveform is used for both the standard (W1) and the electrode-shaping (W7) geometry, the latter shows an increase in efficiency with respect to the former which ranges from $\sim 4\%$ to $\sim 18\%$. This result is consistent with the results reported in [6] for the improved performance achieved with the electrode-shaping geometry. In Fig. 8, we also show the efficiency of the self-erase discharge (W8) and asymmetric pulse (W9) waveforms when applied to the electrode-shaping geometry. The efficiency of these waveforms is significantly higher than the efficiency of the reference waveform at high sustaining voltages. For our simulation conditions, the maximum increase in η (with respect to W1) is found to be $\sim 38\%$ for the self-erase discharge waveform (W8) and $\sim 36\%$ for the asymmetric pulse waveform (W9). In other words, the maximum achievable increase in η is more than doubled when the self-erase discharge waveform (W8) is used instead of the standard waveform on the electrode-shaping geometry. Thus, the simulations suggest that the combination of improved waveform designs with improved

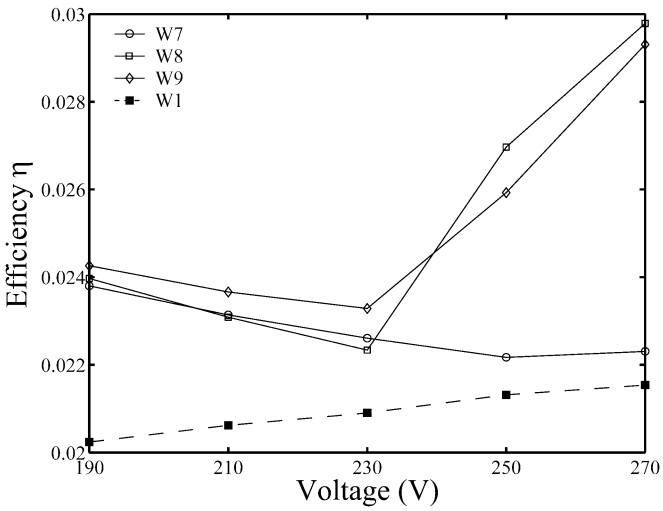

Fig. 8. Visible light generation efficiency η as a function of sustaining voltage V_S for various sustaining waveforms. Results are shown for the electrode-shaping geometry [Fig. 1(b)]. Sustaining frequency is 100 kHz in all cases [$T = 10\ \mu$s in Fig. 2(a) and (b)], and the rise and fall times of all pulses are 100 ns. Dashed line shows the efficiency for our reference waveform W1 (Fig. 3) applied to the standard coplanar-electrode geometry [Fig. 1(a)]. Case W7 corresponds to the reference waveform applied to the electrode-shaping geometry. For waveform W8, we have $T_s = 2.5\ \mu$s, $V_{\rm se} = 0$ V [Fig. 2(a)]. For waveform W9, we have $T_s = 2.5\ \mu$s, $T_1 = 0.2\ \mu$s, $T_2 = 4.8\ \mu$s [Fig. 2(b)].

electrode geometry designs can result in further significant increases in the efficiency of the plasma display.

In Fig. 9(a) and (b), we show the normalized power spent for xenon excitation $\tilde{p}_{\rm exc}$, integrated over time, for the self-erase discharge waveform (i.e., waveform W8 in Fig. 8) and the standard waveform (i.e., waveform W7 in Fig. 8), respectively, applied to the electrode-shaping geometry. We observe that the discharge path is much longer in the waveform W8 case when compared to the reference waveform W7 case. As we mentioned above, the wider the discharge area, the higher the efficiency. We also observe that in the waveform W8 case, the initial discharge path is formed below the inner part of the sustain electrode in the cathode region [snapshot 1 of Fig. 9(a)] but within ~ 5 ns a second discharge path is formed below the outer part of the cathode [snapshots 2, 3 of Fig. 9(a)]. The difference in discharge paths and, consequently, in efficiency is again interpreted based on the surface charge density deposited on the upper dielectric before the initiation of the discharge. In the waveform W8 case, only the portion of the dielectric below the outer part of the cathode is covered with negative charge [Fig. 5(b)], because a self-erase discharge is triggered between the two sustain electrodes that partially erases the surface charge deposited by the previous main discharge.

To get more insight into the physical mechanisms that lead to improved device performance, we note that the calculated increase in the efficiency of the discharge in heating the electrons η_1 is $\sim 21\%$ for the cases shown in Fig. 9. The increase in the efficiency of electrons in producing UV emitting states of xenon η_2 is $\sim 7\%$. The other two factors contributing to the overall efficiency, η_3 and η_4 increase by only $\sim 1\%$ and $\sim 2\%$, respectively. Thus, the wider discharge path results mainly in more efficient heating of the electrons. We also found that the self-erase discharge waveform results in a $\sim 33\%$ reduction in the total dissipated power for the cases shown in Fig. 9.

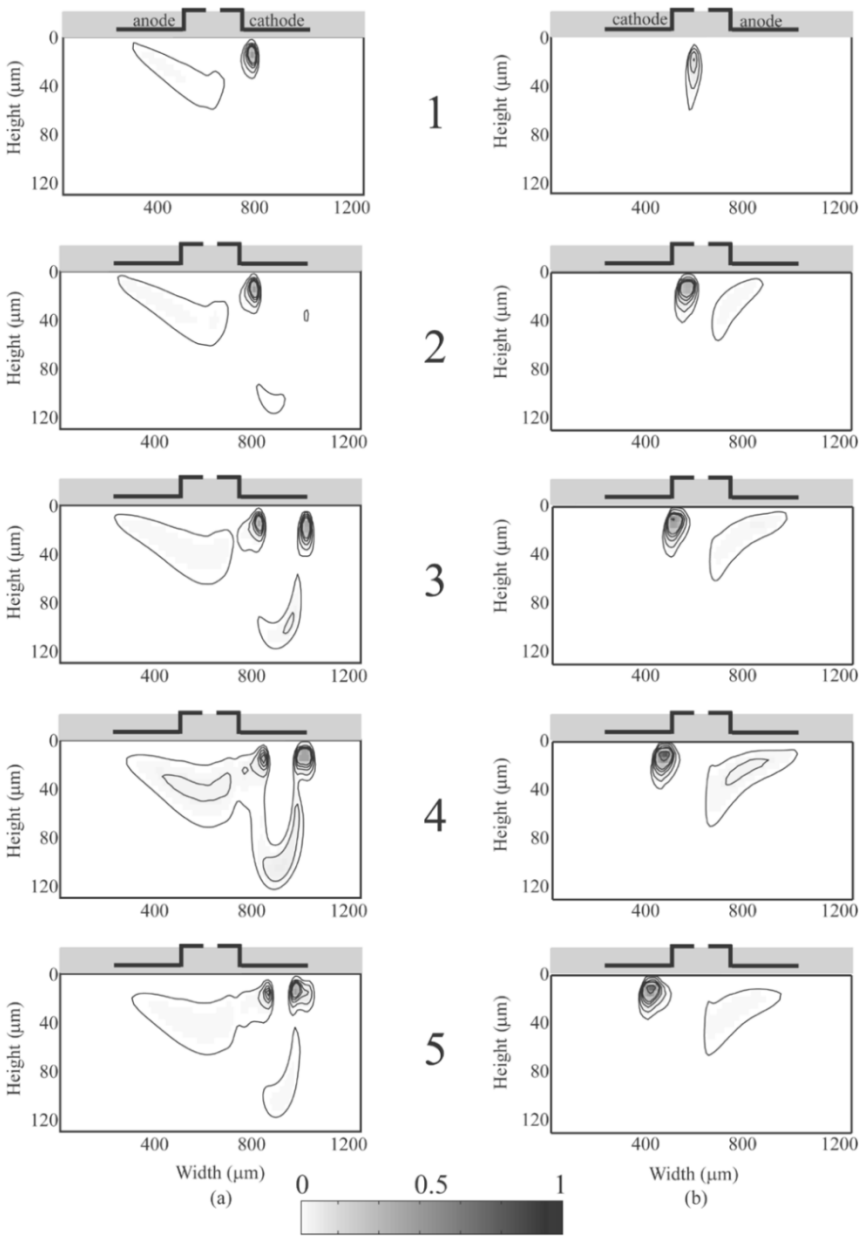

Fig. 9. (a) Normalized power spent for xenon excitation $\bar{p}_{\rm exc}$, integrated over 7.6-ns consecutive time intervals, for the self-erase discharge waveform [Fig. 2(a)] applied to the electrode-shaping geometry [Fig. 1(b)]. Results are shown for waveform W8 (Fig. 8) and $V_S = 270\,\mathrm{V}$. Starting time for integration is 715 ns after the application of a sustaining pulse V_S. (b) Normalized power spent for xenon excitation $\bar{p}_{\rm exc}$, integrated over 7.4 ns consecutive time intervals, for our reference, standard waveform applied to the electrode-shaping geometry [Fig. 1(b)]. Results are shown for waveform W7 [Fig. 8] and $V_S = 270\,\mathrm{V}$. The starting time for integration is 89 ns after the application of a sustaining pulse V_S. Increment between the contours and maximum in gray scale are the same as in Fig. 4(a) and (b). Note the different vertical scale in each plot. In all cases, height is measured from the MgO layer surface.

In the case of the self-erase discharge waveform applied to the electrode-shaping geometry, our simulations suggest that the operation of the cell becomes unstable over a sustaining voltage range within the voltage margin for $V_{se} > 10\,\mathrm{V}$. We found that for the electrode-shaping geometry sufficiently strong self-erase discharges occur even for $V_{se} = 0\,\mathrm{V}$ due to the particular shape of the sustaining electrodes that results in greatly increased surface charge density below their outer part. When this high surface charge density is uncompensated, it results in high electric field and, consequently, intense self-erase discharges even without the electric field of the assistant pulses of magnitude V_{se} [Fig. 2(a)]. It is for this reason that the threshold value of V_{se} for stable operation of the device is much lower in the electrode-shaping geometry compared to the standard geometry. On the other hand, highly efficient designs based on self-erase discharges can be implemented in the electrode-shaping geometry without the need for assistant pulses. In other words, another advantage of the electrode-shaping geometry is that it can operate in the efficient self-erase discharge regime without additional complexity in the waveform design.

IV. Summary and Discussion

We used a 2-D self-consistent simulation model to investigate the effect of several different sustaining voltage waveforms on the visible light generation efficiency of PDP cells. We first

showed that such a model can reproduce all the major trends of previously reported experimental measurements concerning the effect of waveform on PDP efficiency. In addition, all simulation parameters other than the applied sustaining waveform were chosen to be the same for all cases, allowing us to directly compare the different waveforms and their effect on the efficiency. Such a direct comparison could not be done based on the reported experimental data since parameters such as cell dimensions, gas pressure, and sustaining waveform frequency are different in each experiment [13], [14]. The use of the model also allowed us to identify the physical mechanisms that result in higher efficiency.

We also used the 2-D model to suggest new high-efficiency PDP designs. A new sustaining waveform based on a combination of assistant voltage pulses and asymmetric pulse driving resulted in $\sim 25\%$ maximum increase in efficiency within the voltage margin of the cell with respect to the standard sustaining waveform. Combination of the self-erase discharge waveform and electrode-shaping geometry would constitute a new plasma display, which was found to have $\sim 40\%$ maximum increase in efficiency (with respect to the standard waveform and standard geometry) within the voltage margin of the cell.

REFERENCES

[1] A. Sobel, "Television's bright new technology," *Sci. Amer.*, vol. 278, pp. 70–77, May 1998.

[2] S. Matsumoto, *Electronic Display Devices*. New York: Wiley, 1990, pp. 131–131.

[3] J. P. Boeuf, "Plasma display panels: Physics, recent developments and key issues," *J. Phys. D, Appl. Phys.*, vol. 36, pp. R53–79, Mar. 2003.

[4] Y. Sato, K. Amemiya, and M. Uchidoi, "Recent progress in device performance and picture quality of color plasma displays," *J. SID*, vol. 10, pp. 17–23, 2002.

[5] Y. Hashimoto, Y. Seo, O. Toyoda, K. Betsui, T. Kosaka, and F. Namiki, "High-luminance and highly luminous-efficient AC-PDP with DelTA cell structure," *J. SID*, vol. 10, pp. 151–155, 2002.

[6] G. Veronis and U. S. Inan, "Cell geometry designs for efficient plasma display panels," *J. Appl. Phys.*, vol. 92, pp. 4897–4905, Nov. 2002.

[7] S. S. Yang, H. C. Kim, S. W. Ko, and J. K. Lee, "Application of two-dimensional numerical simulation for luminous efficiency improvement in plasma display panel cell," *IEEE Trans. Plasma Sci.*, vol. 31, no. 4, pp. 596–605, Aug. 2003.

[8] J. Ouyang, T. Callegari, B. Caillier, and J. P. Boeuf, "Large-gap AC coplanar plasma display cells: Macro-cell experiments and 3-D simulations," *IEEE Trans. Plasma Sci.*, vol. 31, no. 3, pp. 422–428, Jun. 2003.

[9] G. Oversluizen, M. Klein, S. De Zwart, S. Van Heusden, and T. Dekker, "Discharge efficiency in plasma displays," *Appl. Phys. Lett.*, vol. 77, pp. 948–950, Aug. 2000.

[10] G. Oversluizen, S. de Zwart, S. van Heusden, and T. Dekker, "Dependency of PDP efficacy on gas pressure," *J. SID*, vol. 9, pp. 267–272, 2001.

[11] G. Oversluizen, M. Klein, S. de Zwart, S. van Heusden, and T. Dekker, "Improvement of the discharge efficiency in plasma displays," *J. Appl. Phys.*, vol. 91, pp. 2403–2408, Feb. 2002.

[12] T. Hashimoto and A. Iwata, "Improvement of luminance efficiency in an ACPDP by self-erase discharge waveform," in *SID '99 Dig.*, 1999, pp. 540–543.

[13] S. T. Lo and C. L. Chen, "Improving luminous efficiency of AC-type plasma display panels by adjusting the state of sustaining discharges in the sustaining period," *IEEE Trans. Plasma Sci.*, vol. 30, no. 1, pp. 428–435, Feb. 2002.

[14] J. K. Kim, J. H. Yang, J. H. Seo, and K. W. Whang, "The improvement of discharge characteristics by the use of asymmetric pulse driving in an alternating current plasma display panel," *IEEE Trans. Plasma Sci.*, vol. 29, no. 2, pp. 377–382, Apr. 2001.

[15] S. T. Lo and C. L. Chen, "A new mixed-mode sustain method to improve the luminous efficiency of alternating current plasma display panels," *IEEE Trans. Electron Devices*, vol. 49, no. 5, pp. 762–769, May 2002.

[16] H. S. Tae, K. D. Cho, S. H. Jang, and K. C. Choi, "Improvement in the luminous efficiency using ramped-square sustain waveform in an AC surface-discharge plasma display panel," *IEEE Trans. Electron Devices*, vol. 48, no. 7, pp. 1469–1472, Jul. 2001.

[17] H. S. Tae, B. G. Cho, and S. I. Chien, "Self-erasing discharge mode for improvement of luminous efficiency in AC plasma display panel," *IEEE Trans. Electron Devices*, vol. 50, no. 2, pp. 522–524, Feb. 2003.

[18] J. C. Ahn, Y. Shintani, K. Tachibana, T. Sakai, and N. Kosugi, "Effects of pulsed potential on address electrode in a surface-discharge alternating-current plasma display panel," *Appl. Phys. Lett.*, vol. 82, pp. 3844–3846, Jun. 2003.

[19] J. Kang, O. D. Kim, W. G. Jeon, J. W. Song, J. Park, J. R. Lim, and J. P. Boeuf, "Panel performance of RF PDP," in *Proc. Int. Display Workshops*, 2000, pp. 643–646.

[20] J. Kang, "High luminance and luminance efficiency in PDP's driven by radio-frequency pulses," *J. SID*, vol. 8, pp. 223–226, 2000.

[21] Y. M. Li, C. L. Chen, and H. B. Hsu, "Improve the luminous efficiency of AC plasma display by high-frequency driving on address electrodes," *IEEE Trans. Electron Devices*, vol. 50, no. 4, pp. 913–917, Apr. 2003.

[22] G. Veronis and U. S. Inan, "Simulation studies of the coplanar electrode and other plasma display panel cell designs," *J. Appl. Phys.*, vol. 91, pp. 9502–9512, Jun. 2002.

[23] G. J. M. Hagelaar, M. H. Klein, R. J. M. M. Snijkers, and G. M. W. Kroesen, "Energy loss mechanisms in the microdischarges in plasma display panels," *J. Appl. Phys.*, vol. 89, pp. 2033–2039, Feb. 2001.

[24] W. L. Morgan and B. M. Penetrate, "ELENDIF: A time-dependent Boltzmann solver for partially ionized plasmas," *Comp. Phys. Commun.*, vol. 58, pp. 127–152, 1990.

[25] [Online]. Available: http://www.siglo-kinema.com/database/xsect/siglo.sec

[26] J. Meunier, P. Belenguer, and J. P. Boeuf, "Numerical model of an ac plasma display panel cell in neon–xenon mixtures," *J. Appl. Phys.*, vol. 78, pp. 731–745, Jul. 1995.

[27] G. J. M. Hagelaar, M. H. Klein, R. J. M. M. Snijkers, and G. M. W. Kroesen, "Resonance radiation transport in plasma display panels," *J. Appl. Phys.*, vol. 88, pp. 5538–5542, Nov. 2000.

[28] S. Rauf and M. J. Kushner, "Dynamics of a coplanar-electrode plasma display panel cell. I. Basic operation," *J. Appl. Phys.*, vol. 85, pp. 3460–3469, Apr. 1999.

[29] T. Shinoda, M. Wakitani, T. Nanto, N. Awaji, and S. Kanagu, "Development of panel structure for a high-resolution 21-in-diagonal full-color surface-discharge plasma display panel," *IEEE Trans. Electron Devices*, vol. 47, no. 1, pp. 77–81, Jan. 2000.

[30] W. J. Chung, B. J. Shin, T. J. Kim, H. S. Bae, J. H. Seo, and K. W. Whang, "Mechanism of high luminous efficient discharges with high pressure and high Xe-content in AC PDP," *IEEE Trans. Plasma Sci.*, vol. 31, no. 5, pp. 1038–1043, Oct. 2003.

[31] K. W. Whang and D. C. Jeong, "Observation of the spatiotemporal variation of wall charge distribution in an ac PDP cell," in *SID '03 Dig.*, 2003, pp. 32–35.

G. Veronis (S'00–M'03) was born in Greece on January 11, 1975. He received the B.S. degree in electrical engineering from the National Technical University of Athens, Athens, Greece, in 1997, and the M.S. and Ph.D. degrees in electrical engineering from Stanford University, Stanford, CA, in 1999 and 2002, respectively.

He is currently an Engineering Research Associate at Stanford University.

U. S. Inan (S'76–M'77–SM'99) was born in Turkey on December 28, 1950. He received the B.S. and M.S. degrees in electrical engineering from the Middle East Technical University, Ankara, Turkey, in 1972 and 1973, respectively, and the Ph.D. degree in electrical engineering from Stanford University, Stanford, CA, in 1977.

He is currently a Professor of electrical engineering at Stanford University, where he serves as Director of the Space, Telecommunications, and Radioscience (STAR) Laboratory. He actively conducts research in electromagnetic waves in plasmas, lightning discharges, ionospheric physics, and very low frequency remote sensing. He has served as the Ph.D. thesis adviser for 19 students.

Dr. Inan is a Member of Tau Beta Pi, Sigma Xi, the American Geophysical Union, and the Electromagnetics Academy. He received the 1998 Stanford University Tau Beta Pi Award for Excellence in Undergraduate Teaching. He serves as the current Chair of the United States National Committee of the International Union of Radio Science (URSI) and the International Chair of Commission H (Waves in Plasmas) of URSI.